Utilization of Model Predictive Control to Balance Power Absorption Against Load Accumulation

Preprint

Nikhar Abbas and Nathan Tom
National Renewable Energy Laboratory

Presented at the Annual International Offshore and Polar Engineering Conference (ISOPE)
San Francisco, California
June 25–30, 2017

NREL is a national laboratory of the U.S. Department of Energy
Office of Energy Efficiency & Renewable Energy
Operated by the Alliance for Sustainable Energy, LLC

This report is available at no cost from the National Renewable Energy Laboratory (NREL) at www.nrel.gov/publications.

Conference Paper
NREL/CP-5000-67981
August 2017

Contract No. DE-AC36-08GO28308

NOTICE

This report is available at no cost from the National Renewable Energy Laboratory (NREL) at www.nrel.gov/publications.

Available electronically at SciTech Connect http:/www.osti.gov/scitech

Available for a processing fee to U.S. Department of Energy and its contractors, in paper, from:

U.S. Department of Energy
Office of Scientific and Technical Information
P.O. Box 62
Oak Ridge, TN 37831-0062
OSTI http://www.osti.gov
Phone: 865.576.8401
Fax: 865.576.5728
Email: reports@osti.gov

Available for sale to the public, in paper, from:

U.S. Department of Commerce
National Technical Information Service
5301 Shawnee Road
Alexandria, VA 22312
NTIS http://www.ntis.gov
Phone: 800.553.6847 or 703.605.6000
Fax: 703.605.6900
Email: orders@ntis.gov

Cover Photos by Dennis Schroeder: (left to right) NREL 26173, NREL 18302, NREL 19758, NREL 29642, NREL 19795.

NREL prints on paper that contains recycled content.

Utilization of Model Predictive Control to Balance Power Absorption Against Load Accumulation

Nikhar Abbas, Nathan Tom
National Renewable Energy Laboratory, Golden, CO, USA

ABSTRACT

Wave energy converter (WEC) control strategies have been primarily focused on maximizing power absorption. The use of model predictive control strategies allows for a finite-horizon, multiterm objective function to be solved. This work utilizes a multiterm objective function to maximize power absorption while minimizing the structural loads on the WEC system. Furthermore, a Kalman filter and autoregressive model were used to estimate and forecast the wave exciting force and predict the future dynamics of the WEC. The WEC's power-take-off time-averaged power and structural loads under a perfect forecast assumption in irregular waves were compared against results obtained from the Kalman filter and autoregressive model to evaluate model predictive control performance.

KEY WORDS: Wave energy converter; model predictive control; autoregressive parameterization; wave forecast.

INTRODUCTION

Development of advanced control strategies will be important for the successful implementation of wave energy converter (WEC) technologies. Maximizing power absorption from incident waves has been the primary objective of most previously proposed control algorithms. This work focuses on the development of control algorithms to maximize the power absorption while taking the structural loads on the system into account.

There have been a number of different control strategies investigated in the development of WEC devices. Some of the initial developments in WEC control methods include complex conjugate control (Falnes 2002) and latching control (Babarit and Clément 2006). More complex, constrained control under motion constraints was explored in regular wave examples by (Hals, Falnes, and Moan 2011). Additionally, control using a nonlinear objective function and dynamic models were considered by Nguyen (2016) and Bacelli (2015), respectively. For state-based control algorithms, having knowledge of the incident wave is often considered necessary. One method for attaining this knowledge is through various nonlinear observers and state estimators, such as the extended Kalman filter (Nguyen, Sabiron, Tona, Kramer, and Sanchez 2016; Bernuau, Glumineau, Plestan, and Moussaoui 2015; Fusco and J. V. Ringwood 2013). Model predictive control (MPC) has been shown to improve power production near the theoretical maximum, though computationally demanding (Hals, Falnes, and Moan 2011). One method of forecasting the incident wave excitation force is by using autoregressive models, knowledge of the previous wave history, and the assumption that the change in significant wave height is relatively slow (Fischer, Kracht, and Perez-Becker 2012). Through these techniques, many researchers have developed control algorithms with the focus on maximizing power production at the power take-off (PTO).

An oscillating surge wave energy converter (OSWEC) is under development at the National Renewable Energy Laboratory (NREL). In this report, we focus on maximizing power production while considering the structural loads on the OSWEC through control of the PTO torque. By implementing a variation of the extended Kalman filter, autoregressive parameterization and forecasting, and MPC, a control algorithm that calculates the PTO torque of the OSWEC that is based on the solution to an objective function designed as a quadratic programming problem was developed.

OSWEC AND HYDRODYNAMIC MODELING

The design of the OSWEC used in this study has been detailed in (N. Tom, Lawson, Y.-H. Yu, and Wright 2016a; N. Tom, Lawson, Y. Yu, and Wright 2016b) and is briefly highlighted here. The novel idea in the development of this OSWEC is that the main body has been replaced with identical flaps that can rotate around their horizontal center axis, as shown in Fig. 1. The structural mass is evenly distributed, whereas the structural mass density, ρ_m, is half of the fluid density, ρ. WAMIT (*WAMIT Version 7.0 User Manual* 2014) was used to determine the hydrodynamic coefficients at a step size of 0.01 rad/s for wave frequencies between 0 rad/s and 7.5 rad/s. As mentioned, the aim of this work is to control the PTO torque and not the flap position. The geometric dimensions of the OSWEC used in this study can be seen in Table 1, and the hydrodynamic coefficients can be found in Fig. 2. The hydrodynamic coefficients for other WEC geometries can be found in (N. Tom, Lawson, Y. Yu, and Wright 2016b). A 10 meter water depth was chosen for the hydrodynamic coefficient calculations based on previous studies of fixed-bottom OSWEC systems (Whittaker and Folley 2012; Gomes,

Lopes, Henriques, Gato, and Falcao 2015).

Table 1 Geometric Dimensions of the OSWEC

Water Depth, h, 10 m	Flap Minor Axis, t_f, 1/3 m
Height, H, 10 m	Flap Major Axis, H_f, 2 m
Thickness, t, 3/4 m	Side Support Width, w_s, 1/4 m
Width, w, 20 m	Center of Gravity, r_g, 3.97 m
Flap Width, w_f, 19.5 m	Moment of Inertia, I_{55}, 904.4 kg·m^2
Volume, $\forall$, 72 m^3	Mass, m, 36 t
Resonance Period, T_{res}, 37 s	Resonance Frequency, ω_{res}, 0.17 rad·s^{-1}

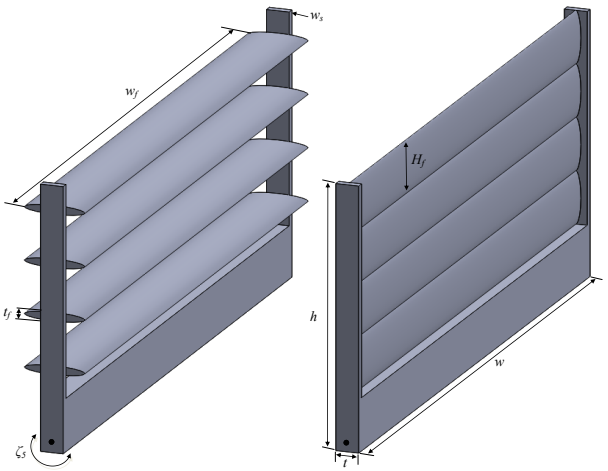

Fig. 1 Solidworks rendering of the novel OSWEC. (Left) Perspective view of the fully open configuration (four flaps open) and (right) perspective view of the fully closed configuration (no flaps open) ζ_5 is the angular displacement of the OSWEC around the axis of rotation.

OSWEC Equations of Motion

To successfully implement an MPC algorithm, the equations of motion for the OSWEC must first be defined.

Continuous Time, Nonlinear Equations of Motion

The one-degree-of-freedom time-domain pitch equation of motion is given by,

$$I_{55}\ddot{\zeta}_5(t) = \tau_{e5}(t) + \tau_{r55}(t) + \tau_h(t) + \tau_d(t) + \tau_m(t) \tag{1}$$

where t is time, I_{55} is the pitch mass moment of inertia, $\ddot{\zeta}_5$ is the pitch angular acceleration τ_{e5} is the wave exciting pitch torque caused by the incident waves, τ_{r55} is the wave radiation torque due to pitch motion, τ_h is the hydrostatic restoring torque, τ_d is the drag torque caused by viscous effects, and τ_m is the mechanical torque applied by the PTO system. With the torque equations defined in (N. Tom, Y. Yu, Wright, and Lawson 2016c), we arrive at the final one-degree-of-freedom pitch equation of motion,

$$\underbrace{(I_{55} + \mu_{55}(\infty))}_{I_t}\ddot{\zeta}_5(t) = \int_{-\infty}^{\infty} K_{e5}(t-\tau)\eta(\tau)d\tau - \int_{-\infty}^{t} K_{r55}(t-\tau)\dot{\zeta}_5(\tau)d\tau - \underbrace{(\rho\forall r_b - mr_g)g}_{C_{55}}\sin(\zeta_5(t)) - \lambda_{vn}|\dot{\zeta}_5(t)|\dot{\zeta}_5(t) + \tau_m(t) \tag{2}$$

where K_{e5} is the wave excitation pitch kernel that is noncausal, and η is the wave elevation. K_{r55} is the pitch radiation impulse response function,

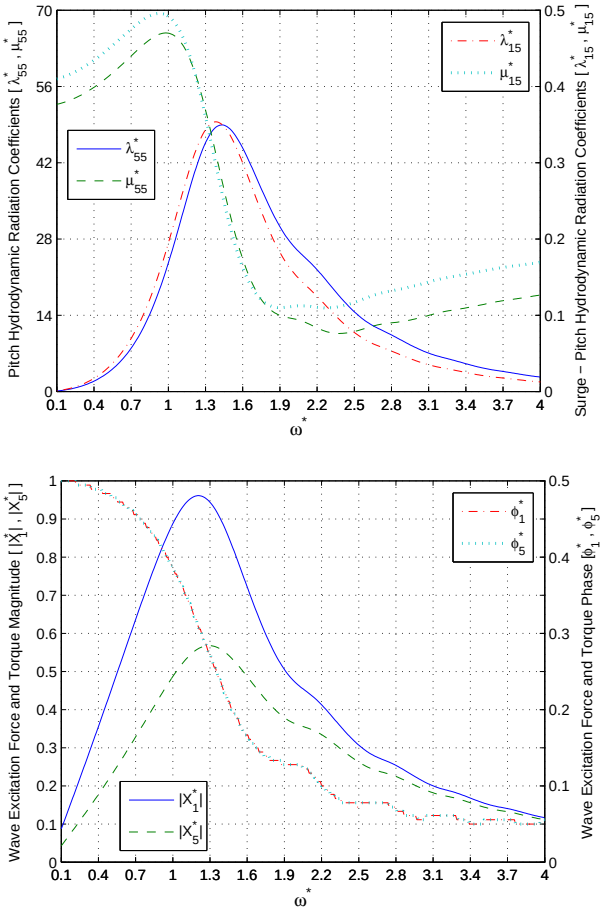

Fig. 2 Nondimensional hydrodynamic radiation (top) and wave excitation (bottom) coefficients. The nondimensionalization is given by: $\omega^* = \omega\sqrt{h/g}$, $\mu^*_{55} = \mu_{55}/I_{55}$, $\lambda^*_{55} = \lambda_{55}/\omega I_{55}$, $X^*_5 = X_5/\rho g h^2 w$, $\mu^*_{15} = \mu_{15}/\rho h^3 w$, $\lambda^*_{15} = \lambda_{15}/\omega\rho h^3 w$, $X^*_1 = X_1/\rho g w h$, $\phi^*_i = \phi_i/\pi$. X^*_1 and X^*_5 are the nondimensionalized surge and pitch wave exciting force coefficients per unit wave amplitude, respectively.

or the memory function, as it represents the wave radiation effects caused by previous OSWEC motions. C_{55} is a constant related to the hydrostatic restoring torque, $\forall$ is the WEC displaced volume in calm water, r_b is the radial distance from the origin to the center of buoyancy, m is the WEC mass, r_g is the radial distance from the origin to the center of gravity, and g is the gravitational acceleration. λ_{vn} is the quadratic-drag coefficient caused by viscous effects, ζ_5 and $\dot{\zeta}_5$ are the angular position and velocity, respectively, and $\mu_{55}(\infty)$ is the added moment of inertia at infinite frequency.

State-Space Formulation

For control application, it is convenient to have the equations of motion in state-space form. It is common to approximate the convolution integral for the wave radiation torque by a linear state-space approximation,

$$\dot{X}_{r55}(t) = A_{r55}X_{r55}(t) + B_{r55}\dot{\zeta}(t) \tag{3}$$

$$\int_{-\infty}^{t} K_{r55}(t-\tau)\dot{\zeta}_5(\tau)d\tau \approx C_{r55}X_{r55}(t) + D_{r55}\dot{\zeta}_5 \tag{4}$$

where $A_{r55}, B_{r55}, C_{r55}, D_{r55}$ are the time-invariant state, input, output, and feed-through matrices, and X_{55} is the state vector describing the convolu-

tion kernel. Generally, D_{55} can be set to zero with minimal effect on the dynamics. Combining (4) with (2), we can establish

$$\ddot{\zeta}_5(t) = \frac{-C_{r55}X_{r55}(t) - C_{55}\sin(\zeta_5(t)) - \lambda_{vn}|\dot{\zeta}_5(t)|\dot{\zeta}_5(t) + \tau_{e5}(t) + \tau_m(t)}{I_t} \tag{5}$$

This defines a nonlinear system described by the continuous time state-space equations

$$\begin{aligned} \dot{x}(t) &= A_{nl}x(t) + B_{nl}u(t) \\ y(t) &= C_{nl}x(t) + D_{nl}u(t) \end{aligned} \tag{6}$$

with state matrices

$$\begin{aligned} A_{nl} &= \begin{bmatrix} A_{r55} & 0 & B_{r55} \\ 0 & 0 & 1 \\ -\frac{C_{r55}}{I_t} & -\frac{1}{I_t\dot{\zeta}_5(t)}C_{55}\sin(\zeta_5) & -\frac{1}{I_t}\lambda_{vn}|\dot{\zeta}_5| \end{bmatrix}, \; B_{nl} = \begin{bmatrix} 0 & 0 \\ 0 & 0 \\ \frac{1}{I_t} & \frac{1}{I_t} \end{bmatrix} \\ C_{nl} &= \begin{bmatrix} 0 & 1 & 0 \\ 0 & 0 & 1 \end{bmatrix}, \; x(t) = \begin{bmatrix} X_{r55}(t) \\ \zeta_5(t) \\ \dot{\zeta}_5(t) \end{bmatrix}, \; u(t) = \begin{bmatrix} \tau_{e5}(t) \\ \tau_m(t) \end{bmatrix} \end{aligned} \tag{7}$$

Linearized System

It is also convenient to have a linearized state space for MPC applications. In this study, we consider the quadratic and nonlinear viscous drag, λ_{vn} to be zero. The small angle approximation allows us to define $\sin(\zeta_5(t)) \approx \zeta_5(t)$. With these definitions, (5) can be linearized to

$$\ddot{\zeta}(t) = \frac{1}{I_t}[-C_{r55}X_{r55}(t) - C_{55}\zeta_5(t) + \tau_{e5}(t) + \tau_m(t)] \tag{8}$$

In the standard, continuous time state-space form,

$$\begin{aligned} \dot{x}(t) &= A_c x(t) + B_c u(t) \\ y(t) &= C_c x(t) + D_c u(t) \end{aligned} \tag{9}$$

a linearized state-space is established

$$\begin{aligned} \begin{bmatrix} \dot{X}_{r55}(t) \\ \dot{\zeta}_5(t) \\ \ddot{\zeta}_5(t) \end{bmatrix} &= \begin{bmatrix} A_{r55} & 0 & B_{r55} \\ 0 & 0 & 1 \\ -\frac{C_{r55}}{I_t} & -\frac{C_{55}}{I_t} & 0 \end{bmatrix} \begin{bmatrix} X_{r55}(t) \\ \zeta_5(t) \\ \dot{\zeta}_5(t) \end{bmatrix} + \begin{bmatrix} 0 & 0 \\ 0 & 0 \\ \frac{1}{I_t} & \frac{1}{I_t} \end{bmatrix} \begin{bmatrix} \tau_{e5}(t) \\ \tau_m(t) \end{bmatrix} \\ \begin{bmatrix} \zeta_5(t) \\ \dot{\zeta}_5(t) \end{bmatrix} &= \begin{bmatrix} 0 & 1 & 0 \\ 0 & 0 & 1 \end{bmatrix} \begin{bmatrix} X_{r55}(t) \\ \zeta_5(t) \\ \dot{\zeta}_5(t) \end{bmatrix} \end{aligned} \tag{10}$$

The continuous time system (9) can be discretized using a zero-order-hold to define

$$\begin{aligned} x(k+1) &= A_d x(k) + B_d u(k) \\ y(k) &= C_d x(k) + D_d u(k) \end{aligned} \tag{11}$$

where

$$A_d = e^{A_c \Delta t} \qquad B_d = A_d^{-1}(A_d - I)B_d \quad \text{if } A_d \text{ nonsingular} \tag{12}$$

$$C_d = C_c \qquad D_d = D_c \tag{13}$$

CONTROLLER DESIGN

A simple block diagram is shown in Fig. 3 to describe the basic control system architecture. There are three primary blocks in the control architecture: an extended Kalman filter with unknown inputs (EKF-UI), autoregressive (AR) model, and MPC. The extended Kalman filter is designed to accept the current OSWEC angular position, $\zeta_5(t)$, velocity, $\dot{\zeta}_5(t)$, and PTO control torque, τ_m, to estimate the wave excitation force in pitch, $\hat{\tau}_{e5}(t)$. The AR model uses the time history of $\hat{\tau}_{e5}$ to define parameters that are used to forecast the incident wave excitation force in pitch $\tilde{\tau}_{e5}$. The calculated $\tilde{\tau}_{e5}$ values are then used in the MPC algorithm to construct an objective function that defines the PTO torque from the current time step to n steps ahead, $\bar{\tau}_m$. The control input calculated for the current time, $\tau_m(k)$, is sent to the OSWEC, and the process is repeated.

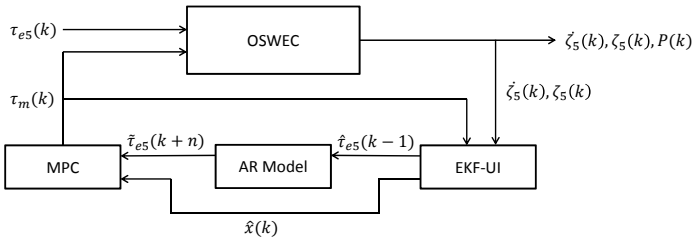

Fig. 3 Simple block diagram showing the basic structure of the control system implemented for the OSWEC

Extended Kalman Filter with Unknown Input

The extended Kalman filter (EKF) method for state estimation requires complete knowledge of the deterministic model inputs. However, these inputs may not always be available. In this study, the primary inputs to the WEC model are τ_{e5} and τ_m. The extended Kalman filter with unknown input (EKF-UI) method, derived in (Ghahremani and Kamwa 2011), presents a solution to state estimation in a nonlinear system with unknown inputs. An overview of the EKF-UI employed in this work is described here; with a continuous time system defined as

$$\begin{aligned} \dot{x} &= f_k(x_k, u_k, u_k^*, w_k) \qquad w_k \sim N(0, Q) \\ y_k &= h_k(x_k, v_k) \qquad v_k \sim N(0, R) \end{aligned} \tag{14}$$

Discretized to

$$\begin{aligned} x_{k+1} &= f_k(x_k, u_k, u_k^*, w_k) \qquad w_k \sim N(0, Q) \\ y_k &= h_k(x_k, v_k) \qquad v_k \sim N(0, R) \end{aligned} \tag{15}$$

where f_k is a nonlinear system function, x_k is a state vector, u_k is the known input, u_k^* is the unknown input, and w_k and v_k represent input and measurement noise, respectively. Finally, y_k is the observed output vector. The noise is assumed to be uncorrelated Gaussian white noise with a normal distribution. The following gradients are first defined:

$$\begin{aligned} F_k &= \left.\frac{\delta f_k}{\delta x}\right|_{\hat{x}_{k|k}} \qquad B_k = \left.\frac{\delta f_k}{\delta u}\right|_{\hat{x}_{k|k}} \qquad L_k = \left.\frac{\delta f_k}{\delta w}\right|_{\hat{x}_{k|k}} \\ H_k &= \left.\frac{\delta h_k}{\delta x}\right|_{\hat{x}_{k|k-1}} \qquad M_k = \left.\frac{\delta h_k}{\delta w}\right|_{\hat{x}_{k|k-1}} \end{aligned} \tag{16}$$

After initialization, there are two primary steps to the EKF-UI. In the measurement update, we correct for errors in the predicted values for the system states (20) and, subsequently, the unknown input value (21). Here we also compute the gain, K_k, and covariance, P_k, matrices of the EKF-UI in equations (17) and (22), respectively. In the time update, the covariance, system state vector, and system outputs are estimated for the next time step in equations (23-25).

Measurement update:

$$K_k = P_k H_k^T (H_k P_k H_k^T + R)^{-1} \tag{17}$$

$$S_k = (B_k^T H_k^T R^{-1}(I - H_k K_k))^{-1} H_k B_k \tag{18}$$

$$e_k = y_k - \hat{y}_{k|k-1} \tag{19}$$

$$\hat{x}_{k|k} = \hat{x}_{k|k-1} + K_k e_k \tag{20}$$

$$\hat{u}_{k-1|k}^* = S_k B_{k-1}^T H_k^T R^{-1}(I - H_k K_k)(e_k + H_k B_{k-1}\hat{u}_{k-2}^*) \tag{21}$$

$$P_{k|k} = (I - K_k H)P_{k|k-1} - K_k H)P_{k|k-1} + (I - K_k) \tag{22}$$

Time update:

$$P_{k+1|k} = F_k P_{k|k} F_k^T + Q \tag{23}$$

$$\hat{x}_{k+1|k} = f_k(x_k, u_k, w_k) \tag{24}$$

$$y_{k+1|k} = h_k(x_k, v_k) \tag{25}$$

From the EKF-UI, the estimated state and unknown inputs calculated in equations (20) and (21) are stored and passed to the AR parameterization and MPC parts of the control algorithm.

Autoregressive Model

An autoregressive model is employed to predict the pitch wave excitation force, τ_{e5}. Equation (26) shows the basic structure of this model

$$\hat{\tilde{y}}(k|\theta) = \phi^T(k)\theta \tag{26}$$

where

$$\hat{\tilde{y}}(k|\theta) = \left[\tilde{\tau}_{e5}(k+1)\ \dots\ \tilde{\tau}_{e5}(k+n)\right],\ \phi^T(k) = \left[\hat{\tau}_{e5}(k)\ \dots\ \hat{\tau}_{e5}(k-n)\right] \tag{27}$$

and θ is a matrix of parameters found through a least-squares minimization. We define $\tilde{\tau}_{e5}$ and $\hat{\tau}_{e5}$ as the wave excitation torque in pitch forecasted by the autoregressive model and estimated by the EKF-UI, respectively.

Model Predictive Control

MPC is used to determine the PTO torque in the OSWEC system. By taking the predicted behavior of the OSWEC into account, the MPC algorithm defines a control input based on a prescribed objective function. In order to do this, the future behavior of the OSWEC must be estimated.

OSWEC Motion Prediction

Beginning with a discrete and linearized state-space equation of motion,

$$\begin{aligned} x(k+1) &= A_d x(k) + B_d u(k) \\ y(k) &= C_d x(k) + D_d u(k) \end{aligned} \tag{28}$$

we define the state-space realization,

$$\begin{aligned} A &= A_d & B &= B_d \\ C &= [0\ 0\ 1] & D &= [0\ 0] \end{aligned} \tag{29}$$

with the state and input vectors, $x(k)$ and $u(k)$:

$$x(k) = \left[X_{55}(k)\ \ \zeta_5(k)\ \ \dot{\zeta}_5(k)\right]^T, \quad u(k) = \left[\tau_{e5}(k)\ \ \tau_m(k)\right]^T \tag{30}$$

We can predict the system output n steps ahead with the following system of equations:

$$\begin{aligned} x(k+1) &= Ax(k) + Bu(k) \\ y(k+1) &= CAx(k) + CBu(k) \\ x(k+2) &= Ax(k+1) + Bu(k+1) \\ y(k+2) &= CA^2x(k) + CABu(k) + CBu(k+1) \\ &\vdots \\ y(k+n) &= CA^nx(k) + CA^{n-1}Bu(k) + CA^{n-2}Bu(k+1) + \dots \\ &\qquad + CA^0Bu(k+n-1) \end{aligned} \tag{31}$$

We can put the equations from (31) into matrix form:

$$\begin{bmatrix} \dot{\zeta}_5(k+1) \\ \vdots \\ \dot{\zeta}_5(k+n) \end{bmatrix} = \underbrace{\begin{bmatrix} CA \\ \vdots \\ CA^n \end{bmatrix}}_{M_1} x(k) + \underbrace{\begin{bmatrix} CB & 0 & \cdots & 0 \\ CAB & CB & \cdots & \vdots \\ \vdots & \ddots & \ddots & 0 \\ CA^{n-1}B & \cdots & CAB & CB \end{bmatrix}}_{M_2} \begin{bmatrix} u(k) \\ \vdots \\ u(k+n-1) \end{bmatrix} \tag{32}$$

It is useful to introduce a permutation matrix P,

$$P = \begin{bmatrix} 1 & 0 & \cdots & 0 & 0 & \cdots & 0 \\ 0 & 0 & \cdots & 1 & 0 & \cdots & \vdots \\ 0 & 1 & \cdots & 0 & 0 & \cdots & \vdots \\ \vdots & \vdots & \ddots & 0 & 1 & \ddots & \vdots \\ \vdots & \vdots & \dots & \vdots & \vdots & \cdots & 1 \end{bmatrix} \in \mathfrak{R}^{n\times 2n} \tag{33}$$

that we can postmultiply M_2 by

$$\dot{\bar{\zeta}} = M_1 x(k) + M_2 P \bar{u} \tag{34}$$

where

$$\bar{u} = \left[\bar{\tau}_{e5}\ \bar{\tau}_m\right]^T = \left[\bar{\tau}_{e5}(k)\ \dots\ \bar{\tau}_{e5}(k+n),\quad \tau_m(k)\ \dots\ \tau_m(k+n)\right]^T \tag{35}$$

so that M_2 is separated into two matrices by the permutation matrix such that

$$M_2 P = \left[M_{21}\ M_{22}\right]$$

and we can arrive at:

$$\dot{\bar{\zeta}}_5 = M_1 x(k) + M_{21}\bar{\tau}_{e5} + M_{22}\bar{\tau}_m \tag{36}$$

It should be noted that $\bar{\tau}_{e5}$ and $\bar{\tau}_m$ consist of torque values from the current time, to the time step $(k+n)$ in the future.

Objective Function for Power Maximization

To define our objective function, we start with the equation for PTO power,

$$P(t) = -\tau_m(t)\dot{\zeta}_5(t) \tag{37}$$

The power maximization at a discrete time step can be presented as

$$\max_{\tau_m(k)} P(k) = \max_{\tau_m(k)} -\tau_m(k)\dot{\zeta}_5(k) = \min_{\tau_m(k)} \tau_m(k)\dot{\zeta}_5(k) \tag{38}$$

Equation 38 presents an interesting problem as the power output of the PTO is a function of both the PTO torque, $\tau_m(k)$, and OSWEC angular velocity, $\dot{\zeta}_5(k)$, at a fixed point in time; however, $\dot{\zeta}_5(k)$ is a direct result of $\tau_m(k-1)$. To maximize time-averaged power, we define an initial objective function (39) for the control algorithm.

$$\min_{\tau_m(tk)} J_p,\ J_p = \sum_{k=1}^{n} \tau_m(k)\dot{\zeta}(k+1) = \bar{\tau}_m^T \dot{\bar{\zeta}}_5 \tag{39}$$

We make the assumption that, with a small enough time step, any errors caused by the difference of time steps in the product used to define the objective function (39) and the product used to calculate the PTO power (37) will be insignificant. Using MATLAB's built-in function, quadprog, (MATLAB 2016) finding the solution to a quadratic programming problem is fairly straightforward. For this reason, we modify (39) to (44),

$$J_p = \bar{\tau}_m^T \dot{\bar{\zeta}} \tag{40}$$

$$J_p^T = x(t)^T M_1^T \bar{\tau}_m + \bar{\tau}_{e5}^T M_{21}^T \bar{\tau}_m + \bar{\tau}_m^T M_{22}^T \bar{\tau}_m, \quad J^T = J \tag{41}$$

$$J_p = [M_1 x(k) + M_{21}\bar{\tau}_{e5}]^T \bar{\tau}_m + \bar{\tau}_m^T M_{22}^T \bar{\tau}_m \tag{42}$$

with

$$f_p = M_1 x(k) + M_{21}\bar{\tau}_{e5}, \qquad Q_p = 2M_{22} = (M_{22} + M_{22}^T) \tag{43}$$

such that

$$J_p = \frac{1}{2}\bar{\tau}_m^T Q_p \bar{\tau}_m + f_p^T \bar{\tau}_m \tag{44}$$

where (44) is the standard form necessary to run MATLAB's quadprog function, and provides an objective function for cumulative absorbed power.

Motion Constraints

It is important to consider constraints on the motion of the OSWEC to keep the control behavior practical and realistic. To do this, we first modify the C matrix from (29) to be

$$C = \begin{bmatrix} 0 & 1 & 0 \end{bmatrix} \tag{45}$$

By applying the same methodology that was used to arrive at (44), we establish a second equation for the predicted angular positions of the OSWEC:

$$\bar{\zeta}_5 = M_{1,mc}\bar{x} + M_{21,mc}\bar{\tau}_{e5} + M_{22,mc}\bar{\tau}_m, \tag{46}$$

Setting the motion constraint $|\bar{\zeta}_5| \leq \xi_(max)$, where ξ_{max} is the angular limit of motion in radians, we can create two equations,

$$\begin{aligned} M_{1,mc}\bar{x} + M_{21,mc}\bar{\tau}_{e5} + M_{22,mc}\bar{\tau}_m &\leq \xi_{max} \\ M_{1,mc}\bar{x} + M_{21,mc}\bar{\tau}_{e5} + M_{22,mc}\bar{\tau}_m &\geq -\xi_{max} \end{aligned} \tag{47}$$

These can be modified to

$$\begin{aligned} M_{22,mc}\bar{\tau}_m &\leq \xi_{max} - [M_{1,mc}\bar{x} + M_{21,mc}\bar{\tau}_{e5}] \\ -M_{22,mc}\bar{\tau}_m &\leq \xi_{max} + [M_{1,mc}\bar{x} + M_{21,mc}\bar{\tau}_{e5}] \end{aligned} \tag{48}$$

which is of the form $Ax \leq b$ where

$$A = \begin{bmatrix} M_{22,mc} \\ -M_{22,mc} \end{bmatrix},\ b = \begin{bmatrix} \xi_{max} - [M_{1,mc}\bar{x} + M_{21,mc}\bar{\tau}_{e5}] \\ \xi_{max} + [M_{1,mc}\bar{x} + M_{21,mc}\bar{\tau}_{e5}] \end{bmatrix} \tag{49}$$

with $x = \bar{\tau}_m$

Torque Penalty

With the initial objective function (44), we can now include an additional term to add a penalty to the amount of torque used by the PTO. This is the simplest way of reducing loads on the system. If we define another objective function,

$$J_\tau = \alpha\bar{\tau}_m^T\bar{\tau}_m \tag{50}$$

where α is a weighting term on the torque penalty.

Foundation Force Reduction

The most direct way of minimizing the loads on the system is to explicitly consider the foundation force in the objective function. Note that this does include the necessity for a prediction of the wave excitation force in surge, f_{e1}. We establish f_{e1} to have a linear relationship to τ_{e5} that is dependent on the sea state, as the two signals are both in phase (Fig. 2). This assumption provided simulation results similar to those performed with a perfect prediction of f_{e1}. Considering the one-degree-of-freedom surge equation of motion,

$$0 = f_{e1}(t) + f_{r1}(t) + f_{r15}(t) \tag{51}$$

where f_{e1} is the wave exciting surge force, f_{r1} is the force required by the foundation to keep the OSWEC stationary, and f_{r15} is the wave radiation force. Equation (51) can be modified to

$$f_{r1}(t) = -f_{e1}(t) - f_{r15}(t) \tag{52}$$

$$f_{r1}(t) = -f_{e1}(t) + \mu_{15}(\infty)\ddot{\zeta}_5(t) + \int_{-\infty}^{t} K_{r15}(t-\tau)\dot{\zeta}_5(\tau)d\tau \tag{53}$$

The second two terms in (53), representing f_{r15} (μ_{15} and convolution integral), can be linearized in a state-space approximation, and the one-degree-of-freedom pitch equation of motion can be put in the discrete state-space form

$$\begin{aligned} A_{sys} &= \begin{bmatrix} A_{r15} & 0 & 0 & B_{r15} \\ 0 & A_{r55} & 0 & B_{r55} \\ 0 & 0 & 0 & 1 \\ 0 & -\frac{C_{r55}}{I_t} & -\frac{C_{55}}{I_t} & 0 \end{bmatrix} \qquad B_{sys} = \begin{bmatrix} 0 & 0 \\ 0 & 0 \\ 0 & 0 \\ \frac{1}{It} & \frac{1}{It} \end{bmatrix} \\ C_{sys} &= \begin{bmatrix} C_{15} & -\mu_{15}\frac{C_{r55}}{I_t} & -\mu_{15}\frac{C_{55}}{I_t} & 0 \end{bmatrix} \quad D_{sys} = \begin{bmatrix} \frac{\mu_{15}}{It} & \frac{\mu_{15}}{It} \end{bmatrix} \end{aligned} \tag{54}$$

where

$$X_{sys} = \begin{bmatrix} X_{r15}\ X_{r55}\ \zeta_5(k)\ \dot{\zeta}_5(k) \end{bmatrix}^T, \qquad u(k) = \begin{bmatrix} \tau_{e5}(k)\ \tau_m(k) \end{bmatrix}^T \tag{55}$$

such that the surge foundation force can now be calculated as

$$f_{r1}(k+1) = -f_{e1}(k) - C_{sys}X_{sys}(k) + D_{sys}u(k) \tag{56}$$

By applying a similar method that was used to derive (36), we can arrive at an equation for the predicted foundation forces, $\bar{f}_{r1}$. Starting with the same method of n step ahead prediction, we can again put the equations in the matrix form

$$\begin{bmatrix} f_{r1}(k+1) \\ \vdots \\ f_{r1}(k+n) \end{bmatrix} = \underbrace{\begin{bmatrix} CA \\ \vdots \\ CA^n \end{bmatrix}}_{N_1} x(k) + \underbrace{\begin{bmatrix} CB+D & 0 & \cdots & 0 \\ CAB & CB+D & \cdots & \vdots \\ \vdots & \ddots & \ddots & 0 \\ CA^{n-1}B & \cdots & CAB & CB+D \end{bmatrix}}_{N_2} \begin{bmatrix} u(k) \\ \vdots \\ u(k+n-1) \end{bmatrix} \tag{57}$$

By using the permutation matrix (33) and defining $\bar{u} = [\bar{\tau}_{e5}\ \bar{\tau}_m]^T$ as in (35), we can reduce this to the following equation describing the predicted foundation force to be reduced,

$$\bar{f}_{r1} = N_1x(k) + N_{21}\bar{\tau}_{e5} + N_{22}\bar{\tau}_m - \bar{f}_{e1} \tag{58}$$

where $\bar{f}_{e1}$ is a vector of predicted wave excitation surge forces. To maintain a convex solution space and ensure optimization of the magnitude of the force, we consider the addition of a penalty term, J_f, to the objective function, J, such that

$$J = J_p + J_\tau + J_f \tag{59}$$

where

$$J_f = \gamma\bar{f}_{r1}^T\bar{f}_{r1} \tag{60}$$

and γ is a penalty term on the foundation force terms. We can expand this based on our derivation of $\bar{f}_{r1}$,

$$\begin{aligned} J_F &= \gamma[N_1x(k) + N_{21}\bar{\tau}_{e5} + N_{22} - \bar{f}_{e1}]^T[N_1x(k) + N_{21}\bar{\tau}_{e5} + N_{22} - \bar{f}_{e1}] \\ &= \gamma[x^T(k)N_1^T + \bar{\tau}_{e5}^TN_{21}^T + \bar{\tau}_m^TN_{22}^T - \bar{f}_{e1}^T][N_1x(k) + N_{21}\bar{\tau_{e5}} + N_{22} - \bar{f}_{e1}] \\ &= \gamma[x^T(k)N_1^TN_1x + + \bar{f}_{e1}^T\bar{f}_{e1} + \bar{\tau}_{e5}^TN_{21}^TN_{21}\bar{\tau}_{e5} + \\ &\quad 2(x^T(k)N_1^TN_{21}\bar{\tau}_e - \bar{f}_{e1}^TN_1x(k) - \bar{f}_{e1}N_{21}\bar{\tau}_{e5}) + \\ &\quad \bar{\tau}_m^TN_{22}^TN_{22}\bar{\tau}_m + 2(x^T(k)N_1^TN_{22} + \bar{\tau}_{e5}^TN_{21}^TN_{22} - \bar{f}_{e1}^TN_{22})\bar{\tau}_m] \end{aligned} \tag{61}$$

and drop the terms that are independent of $\bar{\tau}_m$ because they are not dependent on the solution to the quadratic problem. So we define

$$\begin{aligned} Q_f &= \gamma 2N_{22}^TN_{22} \\ f_f &= \gamma[2(x^TN_1^TN_{22} + \tau_{e5}^TN_{21}^TN_{22} - f_{e1}^TN_{22})]^T \end{aligned} \tag{62}$$

and arrive at a third objective function with a weighting term, γ

$$J_f = \frac{1}{2}\bar{\tau}_m^T(\gamma Q_f)\bar{\tau}_m + \gamma f_f)^T\bar{\tau}_m \tag{63}$$

Objective Function Nondimensionalization

The functions (44), (50), and 50) are three quantities with different units. Because of this, we use the nondimensionalization for J_p, J_τ, and J_f presented in (N. M. Tom, Y.-H. Yu, Wright, and Lawson 2017), and rewrite (59) as

$$J = \underbrace{\frac{J_p}{wP_w}}_{C_w} + \alpha \left| \underbrace{\frac{\bar{\tau}_m}{\frac{1}{6}\rho g h^2 H_a/2}}_{\bar{\tau}_m^*} \right|^2 + \gamma \left| \underbrace{\frac{\bar{f}_{r1}}{\frac{1}{2}\rho g w h H_a/2}}_{\bar{f}_{r1}^*} \right|^2 \tag{64}$$

where C_w is defined as the capture width of the OSWEC. The respective width and height of the OSWEC are w and h, P_w is the time-averaged wave power, and H_a is the average wave amplitude. Equation (64) is the final objective function used in this work.

METHODOLOGY AND RESULTS

The control algorithm has been tested in regular waves to verify controller design, and in irregular waves to evaluate controller performance in a more realistic wave environment.

Regular Wave Analysis

Regular wave analysis is convenient for testing the algorithm to ensure that the desired performance is achieved. We are able to compare the performance of the three aspects of the control architecture in the time domain. It is simple to evaluate any errors in the tracking of τ_{e5} by the EKF-UI (Fig. 4). The autoregressive model forecast should also be accurate in regular waves, as the model needs to define a sine function without any higher order harmonics (Fig. 5). The implementation of the penalty terms, γ and α, to the objective function can be analyzed by looking at the magnitudes of τ_m and f_{r1}(Fig. 7), and the power extraction using MPC can be compared to the theoretical maximums found using a tuned spring-damper control loop (Fig. 6). Considering the relation of the power to the load is important as the overarching goal is to extract as much possible power while minimizing loads. For this purpose, we use the definition for P_{tl}, described in (N. M. Tom, Y.-H. Yu, Wright, and Lawson 2017)

$$P_{tL} = C_w \left(\frac{C_w}{f_{r1}^* + \tau_m^*} \right) \left(\frac{P_O}{\sigma_O} \right) \tag{65}$$

where C_w, f_{r1}^*, and τ_m^* are the nondimensional terms defined in (64), P_O is the time-averaged power absorbed, and σ_O is the standard deviation of this power. In (65), the first term represents the PTO-absorbed power of the OSWEC, the second considers this power with respect to large structure loading, and the third term considers large PTO peak instantaneous power spikes.

Regular Wave Results

Regular wave analysis was done for a wave with a period of 8 seconds and amplitude of 1m. Figure 4 shows good tracking of τ_e by the EKF-UI, after an initialization time of about 40 seconds for both the EKF-UI and the wave train. The error, defined as $\sqrt{(\tau_{e5} - \hat{\tau}_{e5})^2}$, is insignificant after the EKF-UI initialization. With this information, we are then able to use the AR model to define $\tilde{\tau}_{e5}$. As expected, the forecast is nearly perfect, as the signal is oscillating at a fixed amplitude and frequency (Fig. 5). The forecast was done for one period in advance. With accurate implementation of the EKF-UI and forecasting using an AR model, the MPC algorithm is implemented to maximize the PTO-absorbed power of the OSWEC. To validate this, we compare the MPC algorithm to an optimized spring damper control loop that provides the theoretical maximum absorbed power under sinusoidal motion (Falnes 2002).

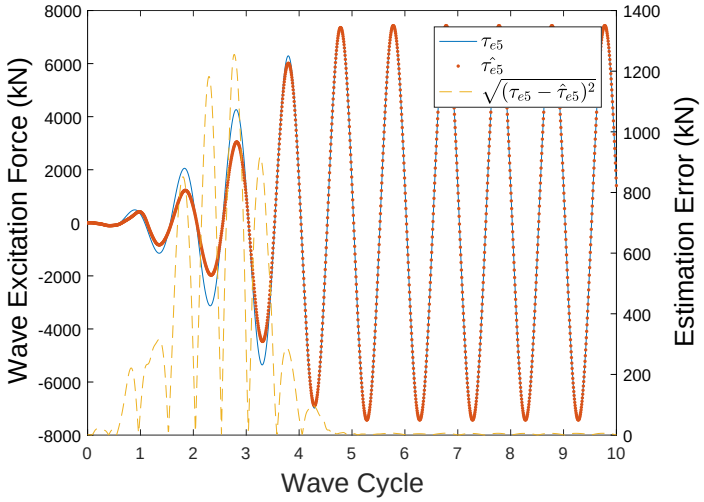

Fig. 4 Actual and estimated wave excitation forces using the EKF-UI in regular waves

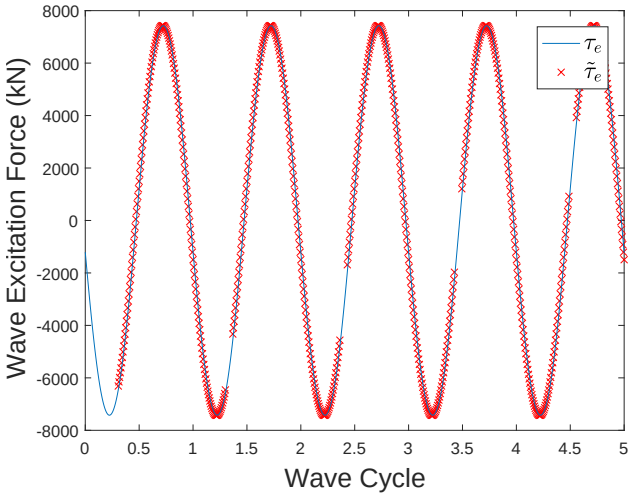

Fig. 5 Actual and forecast wave excitation forces using the AR model. $\tilde{\tau}_{e5}$ is shown periodically in the interest of clarity, but is calculated at every time step.

Figure 6 shows the results of PTO power of the WEC device.

Noticeably, the magnitude of the power fluctuations are less using the MPC algorithm. However, the time-averaged power output using MPC is 4% more than that using the spring-damper control system, before introducing γ and α in the objective function. This increase is most likely because the MPC algorithm does not constrain the OSWEC to sinusoidal motion and is thus able to absorb slightly more power. Associated with the increase of power absorption, the standard deviation of the foundation forces (f_{r1}) and PTO torque (τ_m) are increased by approximately 9% with the implementation of MPC. The nonsinusoidal motion of the OSWEC introduces greater foundation loading and PTO actuation at the peaks of the OSWEC's motion. When implementing γ and α, it is useful to use contour plots to see the penalty term's effect on P_O, σ_{τ_m}, $\sigma_{f_{r1}}$, and P_{tl} (Fig. 7).

As expected, as the penalty term grows, the power output decreases, but so does the actuation effort and loads on the system. In this case, by

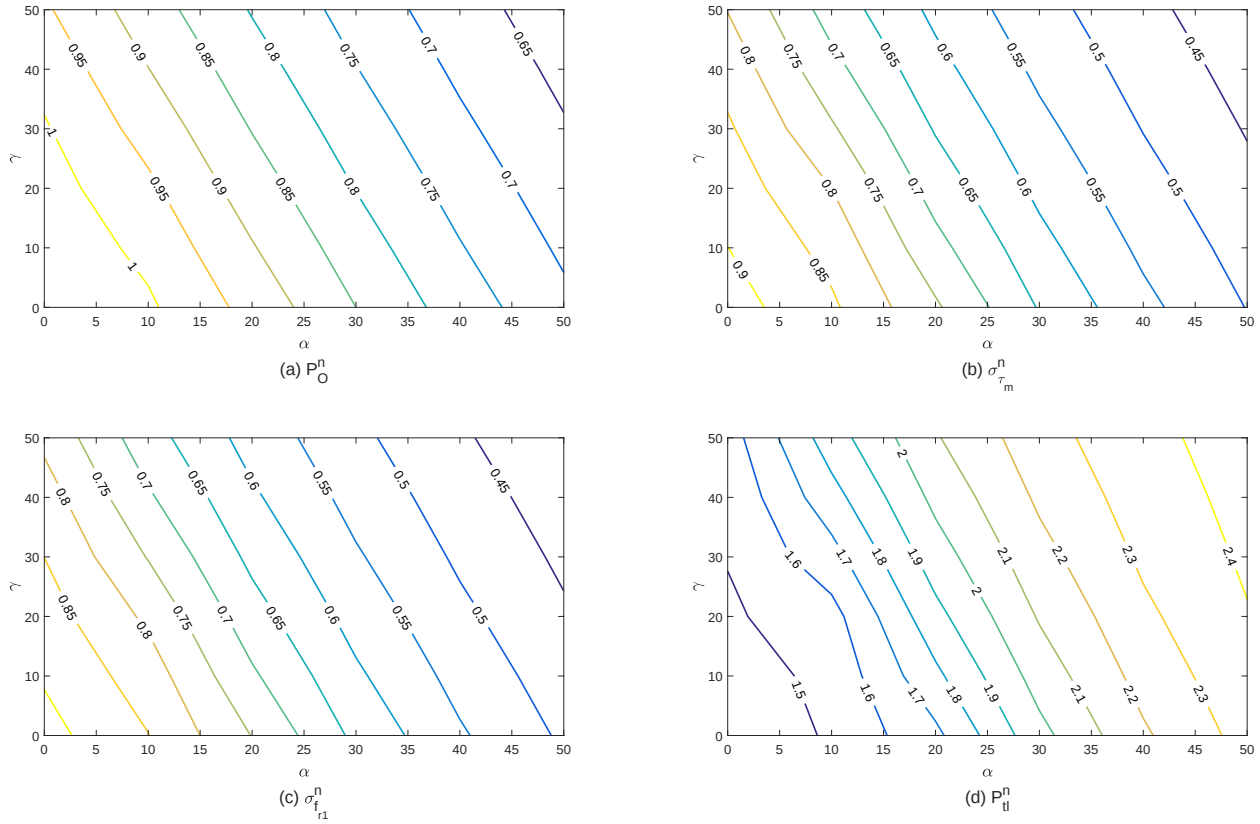

Fig. 7 Contour plots at varied γ and α penalty terms in the MPC objective function (64) with $H = 1$ and $T = 8$. Here, the superscript ^{n} signifies a term normalized by the results using the spring-damper control system.

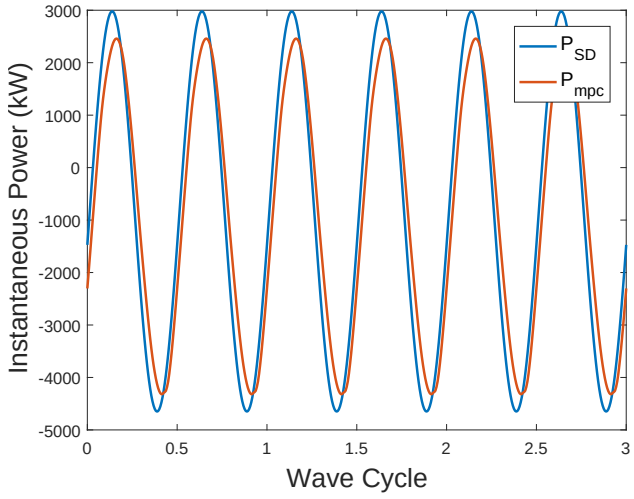

Fig. 6 PTO power for the MPC (P_{mpc}) and spring-damper (P_{SD}) control systems

the definition of P_{tl} in (65), the last contour in Figure 7 suggests that higher α and γ values result in better P_{tl} performance for the range of α and γ values tested. This does not, however, mean that there is not an optimal weighting to maximize P_{tl} if larger α and γ are considered. In irregular waves of varying significant wave heights and frequencies, this relationship can change to differ from the trend seen in Figure 7 and suggests optimal weighting values to maximize P_{tl} within the tested range.

Irregular Wave Analysis

After confirming that this control algorithm is achieving the desired performance in regular waves, we can implement MPC in an irregular wave sea state. For this work, a Bretschneider wave spectrum as defined by **??** was used, where *omega*, ω_m, and H_s are the frequency, modal frequency, and significant wave height, respectively.

$$S(\omega) = \frac{5}{16}\frac{\omega_m^4}{\omega^5}H_s^2 e^{-5\omega_m^4/4\omega^4} \tag{66}$$

It is important to first understand the accuracy of the wave excitation force estimation, ($\hat{\tau}_{e5}$), AR model, and associated forecast of τ_{e5} in irregular waves (Figs. 8, 10). Contour plots that show the power output, standard deviations, $\sigma^n_{\tau_m}$ and $\sigma^n_{f_{r1}}$, and P^n_{tl} at a range of γ and α weightings to evaluate the performance of the MPC algorithm and objective function are shown in Fig. 11 for one sea state. The superscript ^{n} signifies a term normalized by the maximum value using a perfect prediction and no weighting.

Irregular Wave Results

To successfully forecast the incident wave excitation force, the past forces must be accurately estimated. For this, we use the EKF-UI. Figure 8 shows a sample time history, τ_{e5} and $\hat{\tau}_{e5}$, along with the error between the two signals. The EKF-UI takes about 40 seconds to converge to accurately estimate τ_e. After this, the greatest errors seen are $< 1\%$ of the actual wave forces. With the successful estimation of τ_{e5}, we then define an AR model to forecast the incident wave excitation force, $\tilde{\tau}_{e5}$. Figure 10 shows the wave forecasting performance for a sample time

period. Although the wave excitation force forecast is not perfect, the

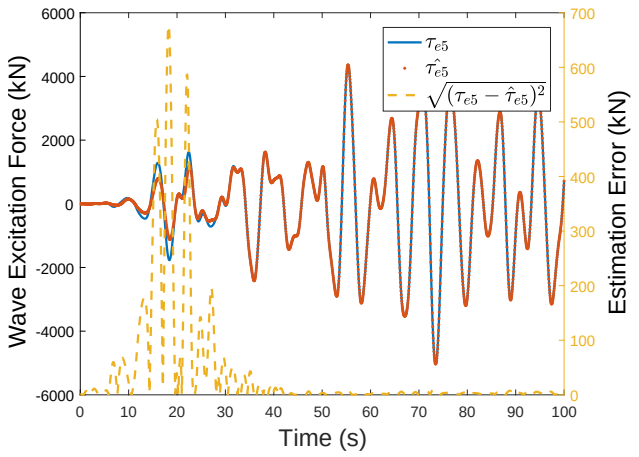

Fig. 8 Actual and estimated wave excitation forces for $H_s = 1m$ and $Tp = 8s$ for the first 100 s of operation

MPC algorithm works well when the AR model to provide a forecast with sufficient accuracy. Figure 9 shows this, especially for shorter peak periods. Interestingly, the mean power output using the AR model to forecast τ_{e5} is greater than that with a perfect forecast for $T_p = 8$. The authors acknowledge that all of the power available may not be absorbed with a perfect forecast of only one peak period ahead. It is possible, in this circumstance, that the AR model forecast is doing a better job of setting up the OSWEC for future wave excitation forces. Careful tuning of the autoregressive order and forecasting horizon may increase the forecast accuracy for longer peak periods. Alternatively, the use of a bank of Kalman filters as suggested in (Nguyen, Sabiron, Tona, Kramer, and Sanchez 2016) may be advantageous. For this work, the forecast horizon time was defined as equal to T_p and the model order was defined as $1.25\frac{T_p}{dt}$, where dt is the length of the discrete time step. A longer forecast horizon or higher model order did not provide better MPC performance.

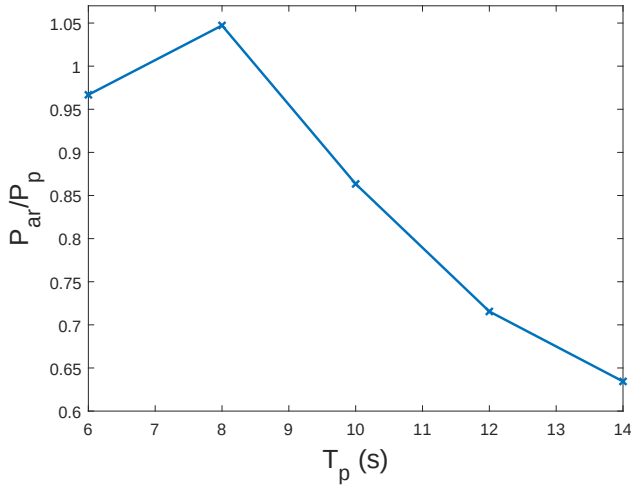

Fig. 9 Normalized power out at varied peak periods (T_p), with H_s = 1m and $\alpha = \gamma = 0$. P_{ar}, and P_p as the average power output, with $\tilde{\tau}_{e5}$ calculated using an autoregressive model or assumed to be perfect, respectively.

Implementation of the penalty terms, γ and α, in the MPC optimization function is displayed in Figure 11 for a significant wave height (H_s) of

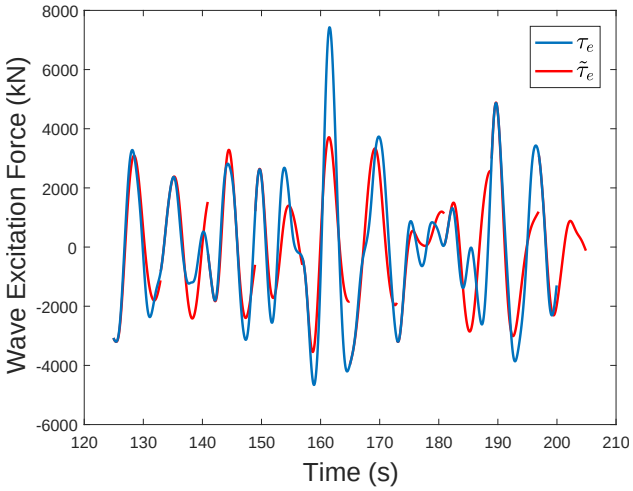

Fig. 10 Forecasted wave excitation force and the actual wave excitation forces for $H_s = 1m$ and $T_p = 8s$. $\tilde{\tau}_{e5}$ is shown periodically in the interest of clarity, but is calculated at every time step.

1 meter and peak period (T_p) of 8 seconds. The addition of weighting terms also contributes to a reduction in P_O^n, $\sigma_{\tau_m}^n$, and $\sigma_{f_{r1}}^n$, as defined in Figure 11, and is mostly consistent with the results observed in regular waves. When considering peak periods ranging from 6 to 14 seconds, the power output at higher peak periods drops along with σ_{τ_m} and $\sigma_{f_{r1}}$, and is consistent with the results in Fig. 9. Additionally, the trends seen in Fig. 11 (a) - (c) are seen in all of the tested wave peak periods. Figure 11(d) suggests that there is are optimal γ and α values to maximize P_{tl}. A shift of the OSWEC's near peak P_{tl}^n in varied sea states is shown in Fig. 12. Similar areas representing the near peak values of the P_{tl}^n contours for a variety of peak periods suggest a shift towards a larger weighting term for longer periods. This shift is likely because the OSWEC may be closer to resonance in longer waves and there is less PTO actuation for power production, so a higher emphasis on the penalty terms is necessary to mitigate loads.

Table 2 Power, torque, and load along near maximum P_{tl} contour

	$P_{O,avg}$	$P_{O,\sigma}$	$\sigma_{\tau_m,avg}$	$\sigma_{\tau_m,\sigma}$	$\sigma_{fr1,avg}$	$\sigma_{fr1,\sigma}$
$T_p = 6$	44.96 kW	8.5%	1.46 Nm	11.3%	0.80 N	11.1%
$T_p = 8$	72.09 kW	9.4%	1.88 Nm	12.2%	1.08 N	12.2%
$T_p = 10$	68.93 kW	8.8%	1.68 Nm	11.1%	0.98 N	11.1%
$T_p = 12$	60.44 kW	6.1%	1.46 Nm	7.5%	0.88 N	7.6%
$T_p = 14$	50.22 kW	4.8%	1.26 Nm	6.0%	0.78 N	5.9%

It should be noted that for any specific peak period, there is a wide range of α and γ values that result in similar P_{tl} performance. Table 2 shows the changes of P, σ_{τ_m}, and $\sigma_{f_{r1}}$ along the contours shown in Figure 12. This table does not show the relation of a specific weighting to another, but rather a percent change in the metric from the minimum to maximum value along the P_{tl} contour. This change suggests that for any specific P_{tl} value, a focus can still be put on power maximization or load minimization in the choice of α and γ, and that weighting function optimization for the OSWEC based on P_{tl} is not absolute. These results do, however, suggest that there is merit in adding a penalty term to the MPC objective function to reduce loads on the system.

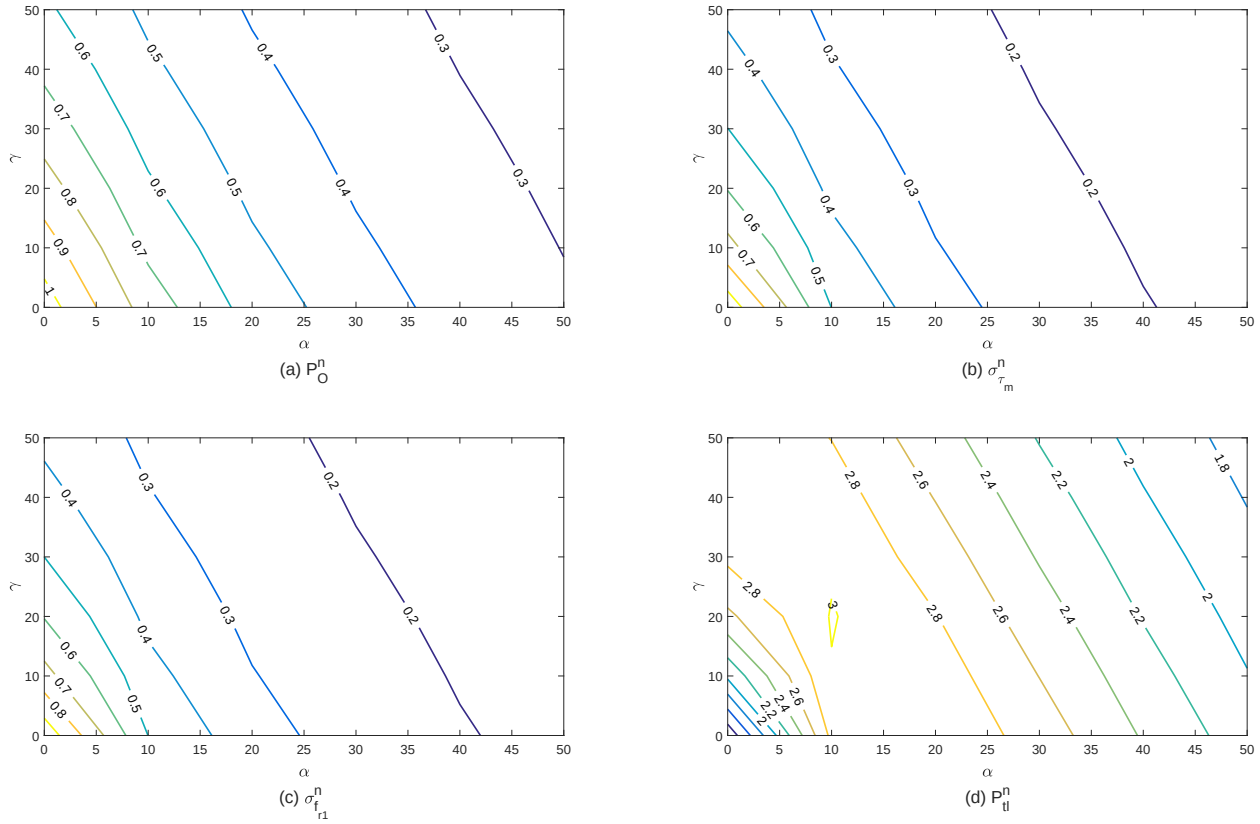

Fig. 11 Contours showing α and γ implementation in irregular waves with $T_p = 8s$ and $H_s = 8m$. The superscript ^{n} signifies a normalized term, in this case by the related simulation output using a perfect prediction without any weighting.

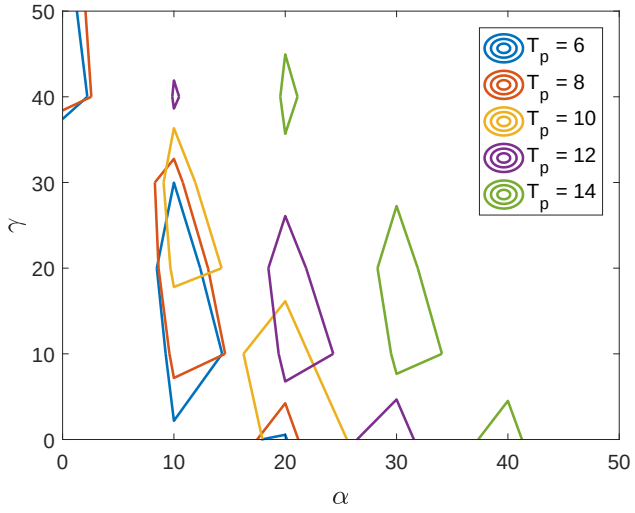

Fig. 12 Contours from near-peak P_{tl} values for irregular waves with peak periods T_p. Maximum P^n_{tl} values are found within each contour, but with a difference from the line displayed.

CONCLUSION

This work has presented a control algorithm for a novel OSWEC that offers the ability to balance the power absorption against the structural loads on the system. An extended Kalman filter with unknown inputs was used to estimate the wave excitation forces on the OSWEC. Using the time history of the estimated wave excitation forces, an AR model was defined and used to forecast the incident wave. The wave forecast was then used in a MPC algorithm to define the torque at the PTO of the OSWEC. The MPC algorithm uses an objective function that includes penalty terms on the control actuation and the foundation forces of the OSWEC. Analysis was done in regular and irregular waves to validate the performance of this work's proposed control system architecture.

The EKF-UI was first tested in regular waves to ensure accurate tracking of the wave excitation force (τ_{e5}). It was found that, after an initialization period, the errors between $\hat{\tau}_{e5}$ as estimated by the EKF-UI and τ_{e5} were near zero (Fig. 4). By applying the estimated wave force, the incident wave forecast was accurate using an AR model (Fig. 5). This response was expected, as the signal to forecast was simply a sine wave. Finally, the performance of the MPC algorithm with and without penalty weights, γ and α, was evaluated in regular waves. Near theoretical maximums were attained using the MPC without any penalty weights. Expected behavior was observed by looking at the contour plots created at different γ and α values. As the weightings were increased, power, torque, and foundation loads decreased. Using this work's definition of P_{tl} (Eq. 65), we found that an increase in penalty weighting was associated with an increase of P_{tl} in regular waves.

The EKF-UI's performance in irregular waves was similar to its performance in regular waves. With accurate tracking of τ_{e5}, the AR model provided adequate forecasting of the incident wave. Although this forecast was imperfect, the controller performance was minimally effected in shorter wave periods wherein the AR model was well defined.

It is possible that more accurate tuning of the AR model in longer wave periods would provide power output values closer to those using a perfect forecast. Consistent results were seen as the weighting terms were increased in the MPC objective function. As with the regular wave results, power, PTO torque, and foundation loads decreased as the weighting terms were increased. The P_{tl} contours (Fig. 12) suggest that it may be beneficial to include a weighting term on the MPC objective function. In doing so, greater power is produced in comparison to the loading of the OSWEC, possibly increasing the life or reducing maintenance costs of the device.

ACKNOWLEDGMENTS

This work was supported by the U.S. Department of Energy under Contract No. DE-AC36-08GO28308 with the National Renewable Energy Laboratory. Funding for the work was provided by NREL's Laboratory Directed Research and Development Program. The U.S. Government retains and the publisher, by accepting the article for publication, acknowledges that the U.S. Government retains a nonexclusive, paid-up, irrevocable, worldwide license to publish or reproduce the published form of this work, or allow others to do so, for U.S. Government purposes.

REFERENCES

Babarit, A. and A.H. Clément (2006). "Optimal latching control of a wave energy device in regular and irregular waves." In: *Applied Ocean Research* 28.2, pp. 77–91.

Bacelli, G., R. Genest, and J.V. Ringwood (2015). "Nonlinear control of flap-type wave energy converter with a non-ideal power take-off system." In: *Annual Reviews in Control* 40, pp. 116–126.

Bernuau, E., A. Glumineau, F. Plestan, and S. Moussaoui (2015). "Finite-time observation and trajectory tracking for a direct wave energy converter." In: *2015 IEEE Conference on Control Applications (CCA)*, pp. 828–833.

Falnes, J. (2002). "Optimum control of oscillation of wave-energy converters." In: *International Journal of Offshore and Polar Engineering*, pp. 147–155.

Fischer, B, P Kracht, and S Perez-Becker (2012). "Online-algorithm using adaptive filters for short-term wave prediction and its implementation." In: *Proceedings of the 4th International Conference on Ocean Energy (ICOE), Dublin, Ireland*. Vol. 1719.

Fusco, F. and J. V. Ringwood (2013). "A Simple and Effective Real-Time Controller for Wave Energy Converters." In: *IEEE Transactions on Sustainable Energy* 4.1, pp. 21–30.

Ghahremani, E. and I. Kamwa (2011). "Simultaneous state and input estimation of a synchronous machine using the Extended Kalman Filter with unknown inputs." In: *2011 IEEE International Electric Machines Drives Conference (IEMDC)*, pp. 1468–1473.

Gomes, RPF, MFP Lopes, JCC Henriques, LMC Gato, and AFO Falcao (2015). "The dynamics and power extraction of bottom-hinged plate wave energy converters in regular and irregular waves." In: *Ocean Engineering* 96, pp. 86–99.

Hals, Jørgen, Johannes Falnes, and Torgeir Moan (2011). "Constrained optimal control of a heaving buoy wave-energy converter." In: *Journal of Offshore Mechanics and Arctic Engineering* 133.1, p. 011401.

MATLAB (2016). *version 9.1.0 (R2016b)*. Natick, Massachusetts.

Nguyen, Hoai-Nam, Guillaume Sabiron, Paolino Tona, Morten Mejlhede Kramer, and Enrique Vidal Sanchez (2016). "Experimental Validation of a Nonlinear MPC Strategy for a Wave Energy Converter Prototype." In: *ASME 2016 35th International Conference on Ocean, Offshore and Arctic Engineering*. American Society of Mechanical Engineers, V006T09A019–V006T09A019.

Tom, Nathan M., Yi-Hsiang Yu, Alan Wright, and Michael Lawson (2017). "Balancing Power Absorption Against Structural Loads with Viscous Drag and Power-Take-Off Efficiency Considerations." In: *IEEE Journal of Ocean Engineering*. Under Review.

Tom, Nathan, Michael Lawson, Yi-Hsiang Yu, and Alan Wright (2016a). "Spectral modeling of an oscillating surge wave energy converter with control surfaces." In: *Applied Ocean Research* 56, pp. 143–156.

Tom, N.M., M.J. Lawson, Y.H. Yu, and A.D. Wright (2016b). "Development of a nearshore oscillating surge wave energy converter with variable geometry." In: *Renewable Energy* 96, Part A, pp. 410–424.

Tom, N.M., Y.H. Yu, A.D. Wright, and M.J. Lawson (2016c). "Pseudo-Spectral Control of a Novel Oscillating Surge Wave Energy converter in Regular Waves, Part I: Power Optimization Including Load Reduction." In: *Ocean Engineering*. Under Review.

WAMIT Version 7.0 User Manual (2014). http://www.wamit.com.

Whittaker, Trevor and Matt Folley (2012). "Nearshore oscillating wave surge converters and the development of Oyster." In: *Phil. Trans. R. Soc. A* 370.1959, pp. 345–364.